Identification of swelling/shrinking coefficients under CO2 on an FKM O-ring – Comparison with HNBR and influence of reinforcements on the matrices

Eric Lainé, Jean-Claude Grandidier, Séverine A.E. Boyer, Benoit Omnès, Fanny Destaing

Matériaux & Techniques **110**, 303 (2022)

https://doi.org/10.1051/mattech/2022029

Matériaux & Techniques

Available online at:
www.mattech-journal.org

REGULAR ARTICLE OPEN ACCESS

Identification of swelling/shrinking coefficients under CO_2 on an FKM O-ring – Comparison with HNBR and influence of reinforcements on the matrices

Eric Lainé[1,*], Jean-Claude Grandidier[1], Séverine A.E. Boyer[1], Benoit Omnès[2], and Fanny Destaing[2]

[1] Institut Pprime, CNRS, ISAE-ENSMA, Université de Poitiers, F-86962 Futuroscope, France
[2] Centre Technique des Industries Mécaniques, F-44308 Nantes Cedex 3, France

Received: 5 January 2022 / Accepted: 22 June 2022

Abstract. A better understanding of elastomers' behavior during Rapid Gas Decompression (RGD) requires advanced knowledge of what is happening during gas sorption and desorption. This will offer to improve numerical simulation phenomena to consider a real environmental use of an O-ring, as for thermal applications. A previous experimental study developed testing protocols to investigate the performance of elastomeric O-rings. The non-contact measurement technique has been validated to identify the swelling and shrinking coefficients during sorption and desorption of carbon dioxide (CO_2) from a Hydrogenated Nitrile Butadiene Rubber (HNBR) O-ring. The present work describes the effect of CO_2 pressures on Fluorocarbon rubber (FKM) seals behavior coupled with temperature. To evaluate the effect of reinforcing the HNBR and FKM matrices with nanofillers, experimental tests were carried out and compared with those of the two elastomers without fillers. The four materials' CO_2 sorption and desorption coefficients are identified, and their swelling upon decompression is measured. It appears that HNBR is the best candidate under the applied service conditions. On the other hand, the nanofillers introduced in the elastomers may cause some early damages under RGD conditions.

Keywords: rubber / coupling environment / CO_2 pressure / material testing / reinforcements

Résumé. Identification des coefficients de gonflement/retrait sous CO2 sur un joint torique en FKM – Comparaison avec le HNBR et influence des renforts sur les matrices. Une meilleure compréhension du comportement des élastomères pendant la décompression rapide des gaz (RGD) nécessite une connaissance avancée de ce qui se passe pendant la sorption et la désorption des gaz. Ceci permettra d'améliorer la simulation numérique de ces phénomènes afin de considérer une utilisation environnementale réelle d'un joint torique, comme pour les applications thermiques. Une étude expérimentale précédente a développé des protocoles d'essai pour étudier la performance des joints toriques en élastomère. La technique de mesure sans contact a été validée pour identifier les coefficients de gonflement et de retrait pendant la sorption et la désorption au dioxyde de carbone (CO_2) d'un joint torique en caoutchouc nitrile butadiène hydrogéné (HNBR). Le présent travail décrit l'effet des pressions de CO_2 sur le comportement des joints en caoutchouc fluorocarboné (FKM) couplé à la température. Pour évaluer l'effet du renforcement des matrices HNBR et FKM avec des nanocharges, des tests expérimentaux ont été réalisés et comparés à ceux des deux élastomères sans charges. Les coefficients de sorption et de désorption sous CO_2 des quatre matériaux sont identifiés, et leur gonflement lors de la décompression est mesuré. Il apparaît que le HNBR est le meilleur candidat dans les conditions de service appliquées. D'autre part, les nanocharges introduites dans les élastomères peuvent entraîner des dommages précoces dans des conditions de RGD.

Mots clés : caoutchouc / environnement de couplage / pression de CO_2 / essais de matériaux / renforcements

* e-mail: eric.laine@ensma.fr

1 Introduction

Carbon dioxide is a natural gas that is frequently encountered in hydrocarbon environments. Relatively low carbon dioxide (CO_2) concentrations in hydrocarbon mixtures can cause significant swelling of the seal. In this context, seals or O-rings must resist and ensure tightness performance throughout their use, although they are prone to the so-called plasticization effect [1]. More significantly, the effect of absorbed CO_2 during a Rapid Gas Decompression (RGD) [2–4] can be catastrophic, and damages depend on parameters, i.e., the decompression speed, the kind of polymer, the squeeze (Parker definition: The squeeze is a ratio of the amount of deformation applied to the seal expressed as a percentage of the free-state cross-sectional thickness), their cure, and the particle reinforcement... Hydrogenated Nitrile Butadiene Rubber (HNBR) and Fluorocarbon rubber (FKM by ASTM standard) are well known for their resistance to RGD and, more generally, to chemical aggression and thermal degradation [5–7]. Saturation conditions, especially in CO_2, are known to alter the gas permeability due to plasticizing effects in almost all polymers, which is more pronounced for elastomer components [8–13]. Besides, they are specially designed for resistance to RGD. Nonetheless, the lifetime sealing performance of polymer materials can be significantly affected when submitted to the gas environment for a long time coupled with high and fluctuating temperatures.

Recently, Haroonabadi et al. [14] stated that the thermal aging (7 days at 100 °C) of NBR vulcanizates depends strongly on crosslink density and mechanical properties. Thermal aging of nitrile rubber samples increased crosslink density and decreased tensile and tear strength, resulting in a decrease in RGD resistance. Thermal aging was studied by Alcock et al. [4] by looking at the effect of exposure to hot air at 150 °C during 12 weeks on the properties of the HNBR compounds with different degrees of carbon black content. The main results are that the permeability decreases following exposure to the hot air of the HNBR samples and that the HNBR samples with the highest carbon black content provide the best barriers to CO_2. Chen et al. [15] investigated the CO_2 diffusivity, solubility, and RGD resistance of HNBR and FKM containing carbon nanotubes. These reinforcements lead to an increase in mechanical properties, reduce CO_2 diffusivity and solubility, and thus improve the RGD resistance of the reinforced elastomers.

Studies of the swelling behavior and, more generally speaking, the volume change phenomenon of elastomers under CO_2 are the most common in literature [5,9,11,16–24]. In addition, the solubility of CO_2 in polymers has been identified by measuring gas sorption [25] using either gravimetric [14,26,27] or spectroscopic methods [28], and has been quantified by direct observation of polymer swelling [27,29,30]. For instance, Ender [31] developed a linear variable differential transformer (LVDT) method to measure O-ring swelling.

Nevertheless, identifying useful diffuso-mechanical properties from O-rings is difficult. One of the first difficulties is related to the geometry of the sample, which is not well suited for classical mechanical tests. If many works exist in the literature, they generally concern materials made in bulk or plates [32,33]. There is always a question about the properties of the O-rings, which are developed with an industrial process that can be slightly different from those of the laboratories. Finally, for identical processes, the polymerization parameters can change in function of the shape and impact the state of the material. Consequently, the present work is motivated by the lack of systematic investigations of CO_2 sorption and desorption through dedicated sealing materials and applications. The challenge is to characterize the behavior directly on the seal and avoid issues about the samples' microstructure compared to those generated by the industrial process.

The second challenge is to realize non-contact measurements in situ in a complex environment. The system couples mechanical tests under temperature and CO_2 pressure control with an in situ optical local deformation measurement that permits to follow the behavior of different elastomers (in the limit hypothesis of small strains). The experimental methodology was revisited to be adapted to seals geometries to be applied as widely as possible [32–35].

This article focuses the study on carbon black filler HNBR and FKM, with and without additional respectively reinforcement with nanofillers, to evaluate the matrices (HNBR, FKM) and the influence of these reinforcements on thermo-diffuso-mechanical characteristics. This work completes the study on the effect of gas on the mechanical behavior of the article [32]. The coupling parameter diffusion swelling and diffusion are extracted from in-situ measurements during solubility-decompression tests. In Section 2, the material and the test bench are described. Then, the in-situ measurement technique is recalled; its complete description has already been described in [33]. Finally, the test protocol [32] is also re-introduced. In Section 3, all the results of the CO_2 sorption and desorption tests at three pressures (2, 4, and 6 MPa) under isothermal conditions (60 and 130 °C) are presented. Comparisons of the results and comments are stated in Section 4. Finally, this work's conclusions and significant results are given in Section 5.

2 Material

2.1 Materials and sample

Two elastomer types, a hydrogenated nitrile rubber (HNBR, Zetpol 2010, Zeon) and a fluoroelastomer type (FKM, FPO3730, Dyneon), were selected for these investigations. The compounds were produced with a nominal hardness of 80 and 90 Shore A, respectively, for HNBR and FKM. They were compounded as summarized in Table 1, using for both a base polymer that is 96% saturated with 36% acrylonitrile content for HBNR and

Table 1. Composition of HNBR and FKM rubbers.

Tableau 1. *Composition des caoutchoucs HNBR et FKM.*

Materials (phr*)	HNBR	HNBR10GE	FKM	FKM10GE
HNBR/FKM	100	100	100	100
N-330 HAF carbon black	70	70	20	20
IMCAL expanded graphite (10GE)		10		10
Antioxidant agent	1.5	1.5	1.5	1.5
Vulcanization agent			8	8
Vulcanizing agent	8	8	2.5	2.5
Vulcanizing accelerator	2	2	3	3

*Parts per hundred rubber parts in weight.

Table 2. Properties in the initial state obtained on each mixing reference.

Tableau 2. *Propriétés dans l'état initial obtenues sur chaque référence de mélange.*

Materials	HNBR	HNBR10GE	FKM	FKM10GE
Density ($g\,cm^{-3}$)	$1.20^{\pm 0.02}$	$1.23^{\pm 0.02}$	$1.88^{\pm 0.02}$	$1.84^{\pm 0.02}$
Hardness DIDC	$81^{\pm 2}$	$85^{\pm 2}$	$84^{\pm 2}$	$91^{\pm 2}$
Hardness Shore A (3 s)	$80^{\pm 2}$	$84^{\pm 2}$	$82^{\pm 2}$	$89^{\pm 2}$
Maximum stress (MPa)	$28.1^{\pm 2.81}$	$23.5^{\pm 2.35}$	$21.5^{\pm 2.15}$	$15.0^{\pm 1.50}$
Stress at 100% (MPa)	$8.4^{\pm 0.84}$	$11.7^{\pm 1.17}$	$7.61^{\pm 0.76}$	$9.03^{\pm 0.90}$
Maximum elongation (%)	$327^{\pm 82}$	$254^{\pm 63}$	$204^{\pm 51}$	$238^{\pm 59}$
DRC à 25 % (%) après 70 h à 150 °C	$45.9^{\pm 2.30}$	$46.2^{\pm 2.31}$	$23.5^{\pm 1.18}$	$28.7^{\pm 1.44}$
Thermal expansion coefficient ($10^{-6}\,K^{-1}$)*	$165^{\pm 8}$	$150^{\pm 8}$	$241^{\pm 8}$	$351^{\pm 9}$

*Average coefficient measured between 20 and 100 °C according to the method described in [33].

70% fluorine content for FKM. HNBR and FKM were vulcanized with peroxide curing systems, respectively dicumyl peroxide and DBPH.

The rubber matrices were reinforced with carbon black and nanofillers. The carbon black reinforcement is fixed at 100 phr. Both matrices were reinforced with 10 phr of nanofiller. The chosen nanofiller was expanded graphite with the reference TIMCAL (Timrex). The chosen denomination is 10GE for each rubber. The rubber compound was obtained with a "classical" compounding operating mode for an elastomer. An internal mixer was used to incorporate the nanofiller. The nanofiller was introduced before carbon black. To improve the homogenization of the compound and avoid delamination defect after curing, for FKM reinforced with nanofiller, two specific processing assistants were used. A specific study was carried out to improve the incorporation of the nanofiller in the rubber matrix. Some difficulties were observed in the first samples, but a correction of the formulation allowed to enhance the quality of the finished part. Furthermore, using GE nanofillers, their better dispersion was observed with the liquid dispersion methodology. The curing process was optimized for each batch to obtain the optimal scorch time and the optimal cure time. Regarding the level of cross-linking density, a slight increase was observed when GE nanofillers were added to the formulation. Table 2 gives the main characteristics for each material, such as density, hardness, maximum stress, and elongation. The average thermal expansion coefficients given in Table 2 for each material were identified using the method described in [33]. This is a DMA (Dynamic Mechanical Analyzer) test in compression. For HNBR, the incorporation of nanofiller reduces tensile strength and elongation at break. For FKM, the incorporation of nanofiller increases the loss factor for high strains. Note that FKM10GE has a lower density than FKM despite the incorporation of reinforcements.

On the other hand, its maximum elongation and thermal expansion coefficient are higher than FKM. This is contrary to what could be expected from the effect of the reinforcements and is not found for HNBR/HNBR10GE. The nominal dimensional characteristics of the O-rings are 50.17×5.33 mm, respectively, in terms of inner diameter and cross-section diameter.

2.2 Experimental device

An Instron 8802 servohydraulic fatigue machine was instrumented with a pressure and temperature regulated chamber, which allows mechanical testing in gaseous nitrogen (N_2), hydrogen (H_2), or carbon dioxide (CO_2) up to 40 MPa and 150 °C. The chamber volume is very limited (1.77 L with a diameter of 150 mm and a length of 100 mm) to ensure the safety related to hydrogen. The device is

amply detailed in previous articles [32,33,36–38]. The particularity of this chamber is to have optical access with a central cylindrical sapphire window of 40 mm diameter at the front and at the back, which allows a complete view.

The O-ring is installed on a rigid U-shaped structure positioned horizontally [32,33] to perform the expansion measurement (thermal and gas). This support is linked to the fixed jaw of the traction machine. Placed on one of the plates, they are free to expand in all three directions, and to facilitate these kinematics; the lower plate is lubricated before the test.

2.3 The technique of dilatation measurement on a seal

The authors have already presented and validated the in-situ strain measurement technique in previous papers [32,33]. It is based on the follow-up of small marks placed on the seal to follow in situ the displacement in a thermo-regulated gas chamber. For metrology, a system of non-contact extensometer is used [32,33]. This method of markers has the advantage of being usable in extreme conditions (high temperatures, high pressures). Four Markers are placed on the O-rings' generatrix, corresponding to the O-ring's parting line projection. The technique consists of following the displacements of each barycenter of the four markers in the plane. To facilitate the analysis, the markers are distributed equidistantly with the following coding: M1 M2 M3 M4. This configuration is chosen to obtain a horizontal measurement of the elongations and gradient by taking them two by two [see [33] for more details]. It is important to note that the camera must be centered between markers M2 and M3 to ensure good quality in the measurements. As markers M1 and M4 are the farthest away, the measurement between these two points incorporates the variabilities and is analyzed with a measurement between markers M2 and M3 closer together. The comparison gives us a first idea of the homogeneity of the deformation field. Two horizontal deviations (noted DevH) are calculated and noted DevH14 and DevH23 respectively in the following part of the paper, and they are defined as follow:
See Equation (1) below

where $X_k^{Mi}, X_k^{Mi}, Y_0^{Mi}, Y_0^{Mi}$ are the current coordinates and initial coordinates of the markers *Mi*.

A secant thermal expansion coefficient is used in the following, then the thermal strain is written as equation (2) following:

$$\varepsilon_{th} = \alpha_{th}(T - T_0), \tag{2}$$

where α_{th} is the secant isotropic thermal expansion coefficient and T_0 is reference temperature. With this secant parameter, the transient phase cannot be represented correctly, as the temperature diffusion cannot be taken into account because of the gradients in the seal during the time. The thermal expansion calculated by equation (2) can be directly compared to the experimental responses.

Similarly, the secant CO_2 swelling (or shrinking) coefficient (α_{CO_2}) is chosen. Finally, a similar expression of the equation (2) is proposed as follows:

$$\varepsilon_{pressure\_CO_2} = \alpha_{CO_2}(P - P_o), \tag{3}$$

where $\varepsilon_{pressure\_CO_2}$ is the strain due to CO_2 pressure. In the remainder of this paper, it is noted "pressure strain". The secant CO_2 swelling (or shrinking) coefficient (α_{CO_2}) defined in equation (3), can be identified with the relation (4):

$$\alpha_{CO_2} = \mathrm{DevH}/(P - P_o). \tag{4}$$

However, temperature couplings can be more complex, and the CO_2 swelling or shrinkage coefficient can be influenced by temperature. Only two temperatures are considered in the test series, so at least the dependence will be regarded as linear. It is important to note that the CO_2 swelling and shrinkage coefficients (or CO_2 sorption and desorption coefficients) are identified similarly to the thermal expansion coefficient. Classically, the volume of an O-ring is calculated using the following simple formula:

$$V^{O-ring} = 2\pi^2 r^2 R, \tag{5}$$

where r is the radius of the cross-section, and the median radius (average of inner and outer radii) is noted R. In this study, an O-ring with the dimensions 50.17×5.33 mm has been investigated. Consequently, parameters r and R have as values respectively 2.665 mm and 27.75 mm. When a volume change of the O-ring appears, radii increase or decrease, according to a thermal condition. More precisely,

$$\mathrm{DevH14}(\%) = \frac{\Delta L}{L_0} = \left(\frac{\sqrt{\left(X_k^{M4} X_k^{M1}\right)^2 + \left(Y_k^{M4} Y_k^{M1}\right)^2}\sqrt{\left(X_0^{M4} X_0^{M1}\right)^2 + \left(Y_0^{M4} Y_0^{M1}\right)^2}}{\sqrt{\left(X_0^{M4} X_0^{M1}\right)^2 + \left(Y_0^{M4} Y_0^{M1}\right)^2}} \right) \times 100,$$

$$\mathrm{DevH23}(\%) = \frac{\Delta L}{L_0} = \left(\frac{\sqrt{\left(X_k^{M3} X_k^{M2}\right)^2 + \left(Y_k^{M3} Y_k^{M2}\right)^2}\sqrt{\left(X_0^{M3} X_0^{M2}\right)^2 + \left(Y_0^{M3} Y_0^{M2}\right)^2}}{\sqrt{\left(X_0^{M3} X_0^{M2}\right)^2 + \left(Y_0^{M3} Y_0^{M2}\right)^2}} \right) \times 100, \tag{1}$$

if it is noted Δr and ΔR the variation of the cross-section radius and the variation of the median radius respectively, due to a thermal increment, then under the assumption of isotropic volume expansion, these variations can be linked with experimental measure:

$$\Delta r = \text{DevH} \times r \text{ and } \Delta R = \text{DevH} \times R. \quad (6)$$

In the end, the volume change (swelling-Sw) due to thermal or CO_2 pressure is determined with this equation:

$$Sw = \frac{V^{O-ring} - V_0^{O-ring}}{V_0^{O-ring}} = (1 + \text{DevH})^3 - 1. \quad (7)$$

It is important to note that the mechanical deformation generated by the mechanical pressure is induced in this measurement. Using an additive law and calculating the mechanical part of the total strain, it turns out that under maximum pressure, the value corresponding to the compression of the joint is 0.02, 0.04, and 0.06% under 2, 4, and 6 MPa of pressure, respectively. These values are lower than the optical measurement accuracy, which depends on the quality of the markers and the optical settings. Taking this effect into account does not change the values of the coupling coefficients in this pressure range.

2.4 Protocol

An identical protocol [32] has been defined to characterize each material. The steps A to G, briefly described here, are applying:

- Step A: Positioning of the seal for compression test on the greased tray;
- Step B: Temperature stabilization at 60 or 130 °C (at least 6 h);
- Step C: Compression tests at isothermal temperature (60 or 130 °C);
- Step D: Pressurization under CO_2 (2, 4, or 6 MPa) at speed between 2 and 4 MPa.min^{-1}, then stabilization for at least 6 h until total gas saturation;
- Step E: Compression tests at isothermal temperature (60 or 130 °C) and constant CO_2 pressure;
- Step F: Back to a zero CO_2 pressure (atmospheric pressure level) at a decompression speed between 2 and 4 MPa.min^{-1}, then stabilization for at least 6 h to obtain the new level of saturation;
- Step G: Compression tests at isothermal temperature (60 or 130 °C).

In the experiment, CO_2 is injected into the chamber with a pump. Initially, it is filled with air at atmospheric pressure. Then, three pressure values are imposed: 2, 4, and 6 MPa in the temperature-controlled chamber, two temperature levels are set. With this protocol, the real pressure (partial pressure Pp) in CO_2 is estimated by taking into account the CO_2 contained in the air with the one added to reach the imposed pressure of 2, 4, or 6 MPa. After all calculations, the corresponding partial pressure in CO_2 is 1.899, 3.899, and 5.899 MPa, respectively [32,33]. To simplify the reading of the paper, only the mechanical pressures are shown.

The choice of CO_2 pressure and temperature values corresponds with NACE TM0192-98 [39] and NORSOK M710 [40], and under NACE TM0192-98 conditions, where the pressure is level is proposed to be 5.2 MPa under an ambient temperature. In the NORSOK M710 standard, the impact of temperature and pressure on the diffusion effect is apprehended by increasing the values to 130 °C and 6 MPa. It is important to note that the thermal resistance of the HNBR dictates the temperature limit. Besides, it should be pointed out that the machine imposes the decompression rate during these tests. The decompression rate cannot be controlled. However, the average depressurization rate is around 2 MPa.min^{-1}.

3 Results

3.1 CO_2 sorption tests under isothermal conditions

Six different seals with material FKM, HNBR10GE, and FKM10GE under the conditions of temperature (60 and 130 °C) and CO_2 pressure (2, 4, and 6 MPa) are tested. In addition, HNBR seal, CO_2 pressurization tests have been performed before [33] and added in Figure 1 to analyze the results. All horizontal deviations are plotted in Figure 1 as a function of the time root during CO_2 pressurization, respectively, at 60 and 130 °C. The transient curves, i.e., before stabilization, have characteristic times identical to the diffusion and give the same response. Comparison of characteristic times shows that the more the pressure is important, the less the transient phase is prolonged.

After several tests, it turns out that the measurement errors on the deviations are in the order of 2 to 5% depending on the level of pressure applied. Despite the experimental complexity, the analysis of the images allows us to obtain measurements that are pretty precise since they will enable us to quantify the fluctuations in the expansion of the joint induced by the slight temperature oscillations imposed by the enclosure during the test. These fluctuations are caused by the regulation of the thermal system. They lead to a modulation in solubility coupled to thermal gradients. By comparing the responses of the two temperatures tested, the increase in the deviation during the pressurization phase under CO_2 reflects perfectly the effect of the temperature on the absorption phase and solubility. Looking at Figure 1, it is clear that the four materials do not behave in the same way when pressurized with CO_2. The stability time and sorption coefficients in this phase are different and will be discussed more precisely in the following paragraph.

3.2 CO_2 desorption tests under isothermal conditions

Systematically on each solubility test at different pressures, measurements during the CO_2 desorption phase are carried out to evaluate the irreversible effects generated by the gas diffusion inside the rubber. The purpose is to know to what extent the behavior of the four seals (HNBR, FKM, HNBR10GE, and FKM10GE) has been modified or not by the CO_2 absorption phase at a given pressure. The deviations are also measured for each temperature during

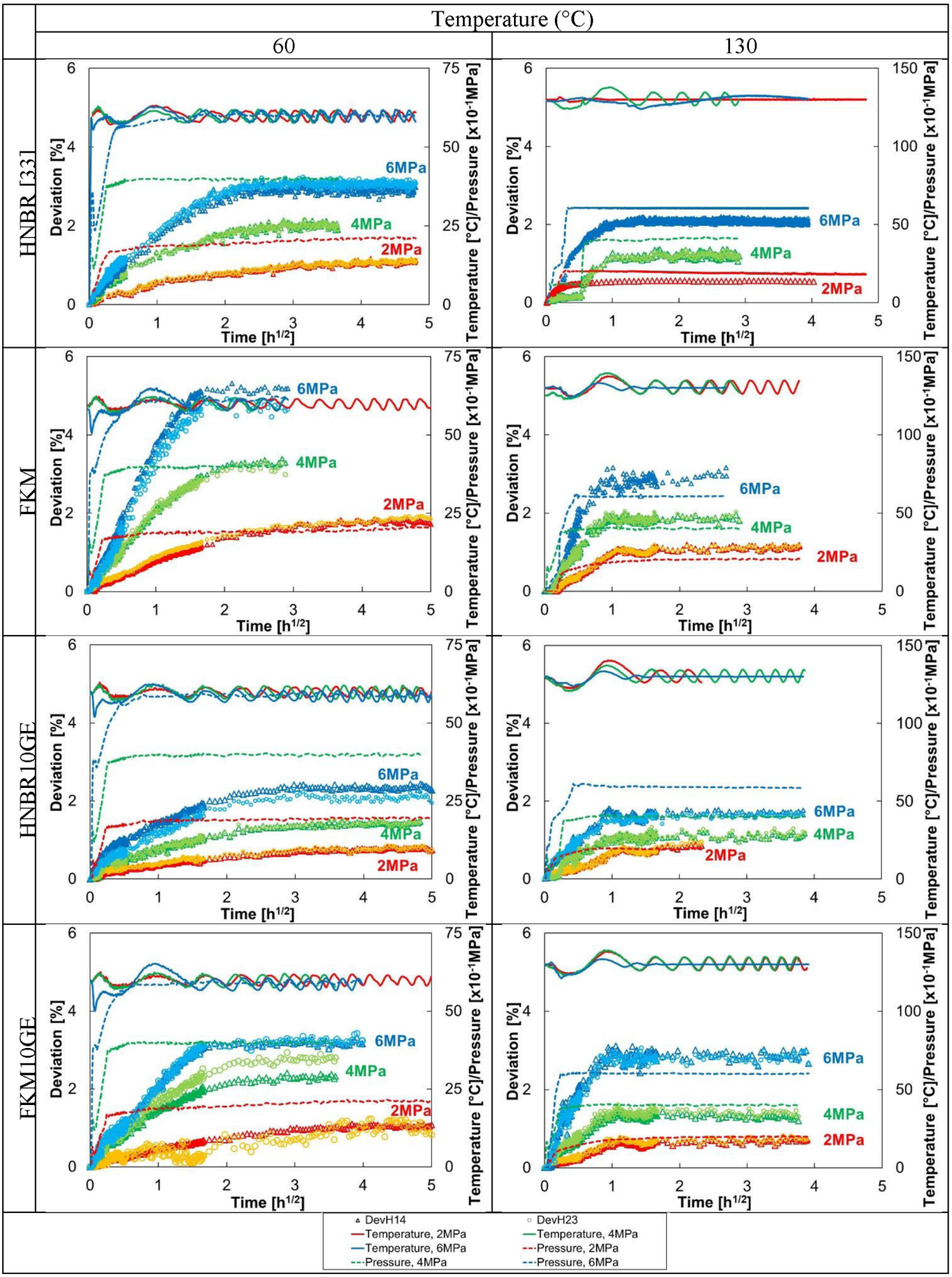

Fig. 1. CO_2 sorption tests at different CO_2 pressures (2, 4, and 6 MPa) at 60 and 130 °C.

Fig. 1. *Essais de sorption sous CO_2 à différentes pressions de CO_2 (2, 4, et 6 MPa) à 60 et 130°C.*

the whole CO_2 depressurization phase until the return to ambient air and stabilization. Figure 2 shows the deflection responses at 60 and 130 °C, respectively, for each system. In the respective Tables 1A–4A (see Appendix), the values of the deviations measured after stabilization are given. The CO_2 shrinking coefficients were calculated from equation (4) for each test condition (initial temperature and pressure) for HNBR, FKM, HNBR10GE, and FKM10GE, respectively.

In general, the curves in Figure 2 show a transient diffusion-type response within some cases substantial variations during the decompression phase. The responses are strongly dependent on material type, saturation pressure, and temperature, revealing a complex behavior during the RGD phase. The deviation does not return to zero, and the higher the saturation pressure, the greater the residual deviation.

4 Discussions

4.1 Saturation time

Histograms of saturation time as a function of ΔP_{CO_2} at 60 °C (Fig. 3a) and 130 °C (Fig. 3b) show that these specific times are different, depending on the materials and the temperature. Thus, globally between 60 and 130 °C, the saturation time is strongly reduced (for 2 and 6 MPa respectively from 87.5% and from 5 to 75% depending on the material). At 60 °C, the effect of the imposed pressure is very marked; the saturation time decreases with the increase in pressure. On the other hand, this effect is weak at 130 °C. If at 60 °C and 2 MPa, the four materials have almost the same saturation time, for the other two pressures, it appears that HNBR saturates less quickly than FKM. This is also true at 130 °C and for all three pressures. Finally, while the reinforcements seem to delay saturation at 60 °C, this is not the case at 130 °C.

4.2 Swelling during CO_2 depressurization

A few seconds or minutes after depressurization, some seals inflated depending on the initial pressure and temperature conditions before returning almost to their initial situation. Table 3 shows the percentage of swelling, calculated according to equation (7), for each material at the initial (nominal) conditions.

HNBR seal swells during decompression at two temperatures only for the initial pressure of 6 MPa. At 60 °C, the HNBR seal shows a maximum deviation of about 7.69% after 16 minutes following the depressurization phase, which corresponds to 24.90% swelling. After 2 h 45, the O-ring returns to its initial position. After more than 22 h, the deviation stabilizes. At 130 °C, during the 6 MPa depressurization, the maximum deviation is 0.75% which corresponds to 2.27%, recorded 12 minutes after depressurization.

For the FKM seal, when depressurizing from 4 and 6 MPa at 60 and 130 °C, it starts to swell very quickly, even before the depressurization is completed. At 60 °C, after 123 s, the maximum deviation measurement is 12%, which corresponds to 40.50% of swelling. At 130 °C, the maximum average deviation is 2.27% or 6.96% swelling at 280 s. FKM seal returns to its initial geometry, before depressurization, at 60 and 130 °C at 409 and 326 s, respectively. As with HNBR, the swelling decreases with increasing temperature. On the other hand, the swelling at the time of depressurization to 6 MPa is much faster than for HNBR. Moreover, the time to recover its initial geometry is completely different between the two materials. For the desorption test in the HNBR10GE seal at 6 MPa and 130 °C, the data acquisition was lost quickly due to the swelling elastomer seal and, consequently, its damage (see Sect. 4.4).

For FKM10GE, during the test (4 MPa, 60 °C), it was impossible to measure the deviations due to a problem of data acquisition. In these conditions, the FKM10GE seal shows a maximum deviation of about 9.08% after less than 2 minutes of depressurization at 6 MPa, corresponding to 29.78% of swelling. Within 4 h following, the seal returned to its initial position; the deviation was stabilized. The stabilization time for a 2 MPa depressurization is about 16 h. At 130 °C, during the 6 MPa depressurization, the maximum deviation is 6.96%, which corresponds to 22.35% of swelling.

4.3 HNBR and FKM rubber matrices

The CO_2 compression tests carried out on HNBR, and FKM seals had been shown in articles [32,33]. FKM appears more rigid than HNBR in the initial state (in the air), but it becomes less rigid than HNBR after a stage under 2 MPa CO_2 pressure. FKM is therefore much more affected by CO_2 than HNBR.

In Figure 4 are plotted the measurement of the "local deformation" or deviation (DevH) (Eq. (1)) as a function of the variation of the pressure ΔP_{CO_2} (see Sect. 2.4) corresponding to each pressure (2, 4, and 6 MPa). For CO_2 sorption and desorption at 60 and 130 °C for (a) HNBR and (b) FKM, linear relationships are representative of the material RGD behavior in this range of pressure. For HNBR at 60 °C, the sorption deviations for 2, 4, and 6 MPa are respectively 1.0, 1.9, and 2.9% (Fig. 4a, Table 1A [see Appendix]). On the other hand, at 130 °C, they are about 40% lower than at 60 °C; the percent difference seems to increase with pressure or ΔP_{CO_2} of 2, 4, or 6 MPa. For FKM at 60 °C, the sorption deviations for 2, 4, and 6 MPa are respectively 1.9, 3.2, and 4.8% (Fig. 4b, Table 2A [see Appendix]). On the other hand, at 130 °C, they are about 40–41% lower than at 60 °C, with a slight difference in percent increase with pressure. Desorption deviations for both HNBR and FKM show similar tendencies. We can notice that the linear regression calculation passes through zero (sorption: at 0 MPa, no swelling occurs, desorption: it is estimated that the CO_2 is completely released from the materials). For both temperatures (Fig. 4), the CO_2 swelling (or sorption) coefficients are independent of the pressure. For HNBR, the average values at 60 and 130 °C are 4.83×10^{-3} MPa^{-1} and 3.12×10^{-3} MPa^{-1}, respectively. For FKM, the average values at 60 and 130 °C are 8.13×10^{-3} MPa^{-1} and 5.05×10^{-3} MPa^{-1}, respectively.

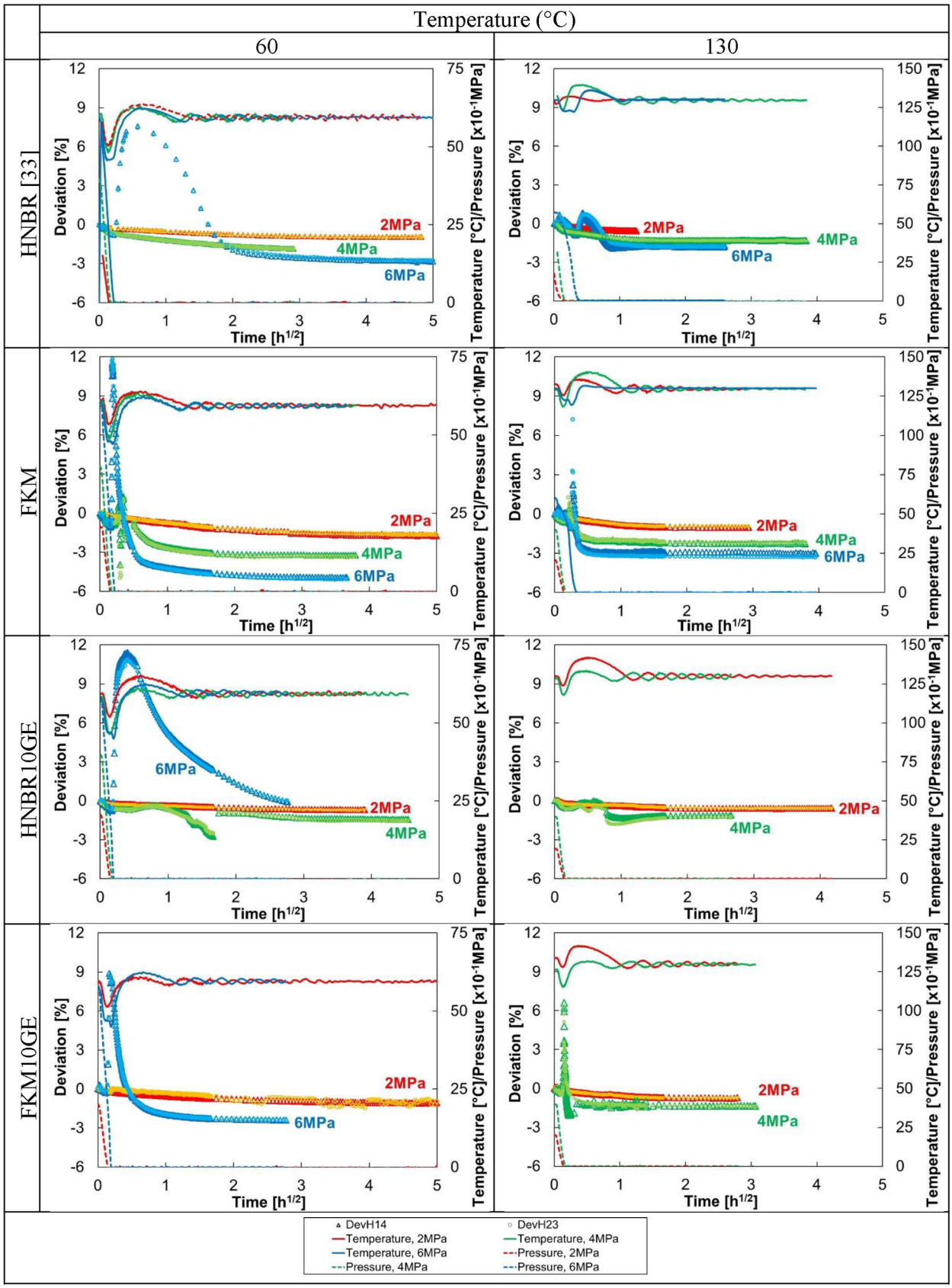

Fig. 2. CO_2 desorption tests at different CO_2 pressures (2, 4, and 6 MPa) at 60 and 130 °C.

Fig. 2. *Essais de desorption sous CO_2 à différentes pressions de CO_2 (2, 4, and 6 MPa) à 60 et 130°C.*

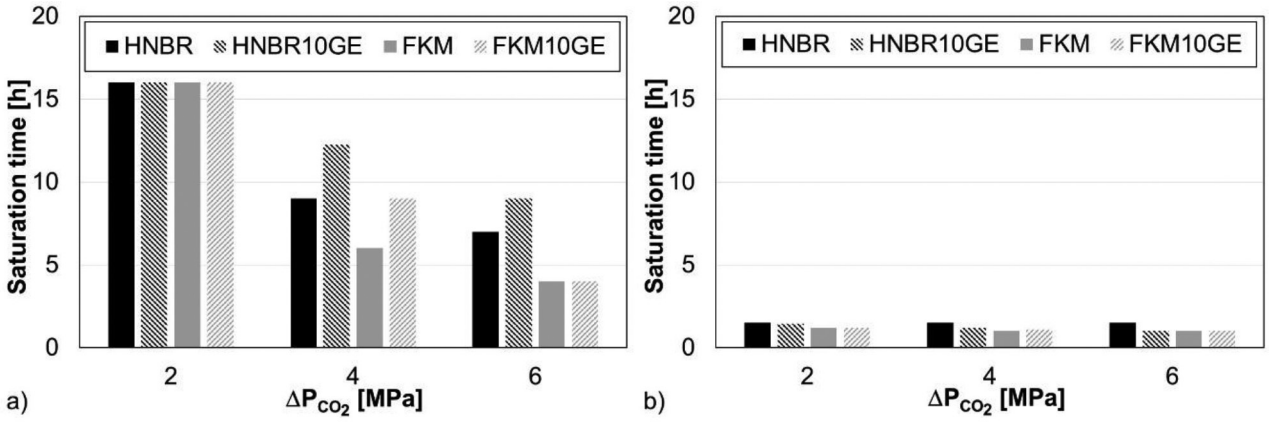

Fig. 3. Saturation time a function of ΔP_{CO_2}. (a) 60 °C; (b) 130 °C.

Fig. 3. *Temps de saturation en function de* ΔP_{CO_2}. *(a) 60°C; (b) 130°C.*

Table 3. Values of the maximum swelling elastomer seal (%) according to the initial (nominal) conditions applied.

Tableau 3. *Valeurs du gonflement maximal du joint élastomère (%) en fonction des conditions initiales (nominales) appliquées.*

Temperature (°C)	60			130		
Pressure (MPa)	2	4	6	2	4	6
HNBR	NO	NO	24.90% 929 s	NO	NO	2.27% 687 s
HNBR10GE	NO	NO	37.95% 640 s	NO	NO	Not measured
FKM	NO	4.04% 443 s	40.49% 123 s	NO	4.72% 151 s	6.96% 280 s
FKM10GE	NO	Not measured	29.78% 106 s	NO	22.35% 81 s	Not measured

4.4 Effects of 10GE reinforcements on HNBR matrix

Figure 5a (Table 3A [see Appendix]) illustrates the deviations as a function of the pressure variation of CO_2 for the different pressures and at the two temperatures for HNBR10GE. The deviations values obtained during sorption and desorption are presented. A linear regression of the deviation as a function of the pressure is made for each configuration and allows to identify the coefficients of sorption and desorption. The desorption coefficients at 60 and 130 °C are identified only from the measurements at 2 and 4 MPa. In the 6 MPa tests, the swelling of the seal at the start of decompression caused damage to the markers and thus the loss of optical measurement monitoring. For HNBR10GE at 60 °C, the sorption and desorption coefficients are $3.75 \times 10^{-3}\,MPa^{-1}$ and $3.66 \times 10^{-3}\,MPa^{-1}$, respectively, in the stabilization phase. At 130 °C, these coefficients are respectively $2.93 \times 10^{-3}\,MPa^{-1}$ and $3.01 \times 10^{-3}\,MPa^{-1}$. Between 60 and 130 °C, the sorption and desorption coefficients decrease by approximately 22 and 18%, respectively. Therefore, the determination of the desorption coefficients at 60 and 130 °C only from 2 and 4 MPa is reasonable because these values are very close to those determined for the sorption on the range 2 at 6 MPa.

In Figure 5b, the average values between of the sorption and desorption coefficients are compared for the two temperatures for HNBR and HNBR10GE. The effect of the fillers is not negligible at 60 °C because the sorption-desorption coefficient drops by about 22.82%. The nanofiller, therefore, prevents the HNBR matrix from swelling. Nanofiller improves barrier property by creating obstacles in the path of penetration of the gas. At 130 °C, the difference between the coefficients is only 4.08%. Thus, the nanofiller had a minimal influence at this temperature. Stiffening the HNBR matrix with nanofillers prevents gas from penetrating the polymer. This is especially true at 130 °C, as it is known that HNBR is more incompressible.

For HNBR10GE, blisters appeared in the following configurations: at 60 °C and 130 °C, 4 and 6 MPa [32]. On the other hand, at 60 °C and 6 MPa, only small blisters (Fig. 6a) appeared during the decompression stage. For other conditions, the swelling was much more critical. At

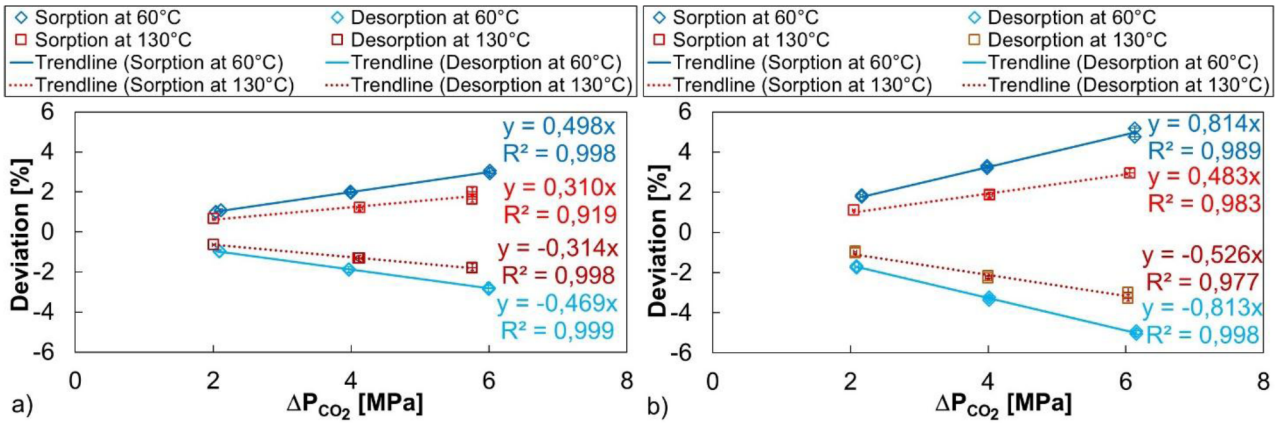

Fig. 4. Deviation as a function of ΔP_{CO_2}. Determination of CO_2 sorption and desorption coefficients at 60 and 130 °C for (a) HNBR and (b) FKM.

Fig. 4. *Déviation en fonction de la* ΔP_{CO_2}. *Détermination des coefficients de sorption et de désorption du* CO_2 *à 60 et 130 °C pour (a) le HNBR et (b) FKM.*

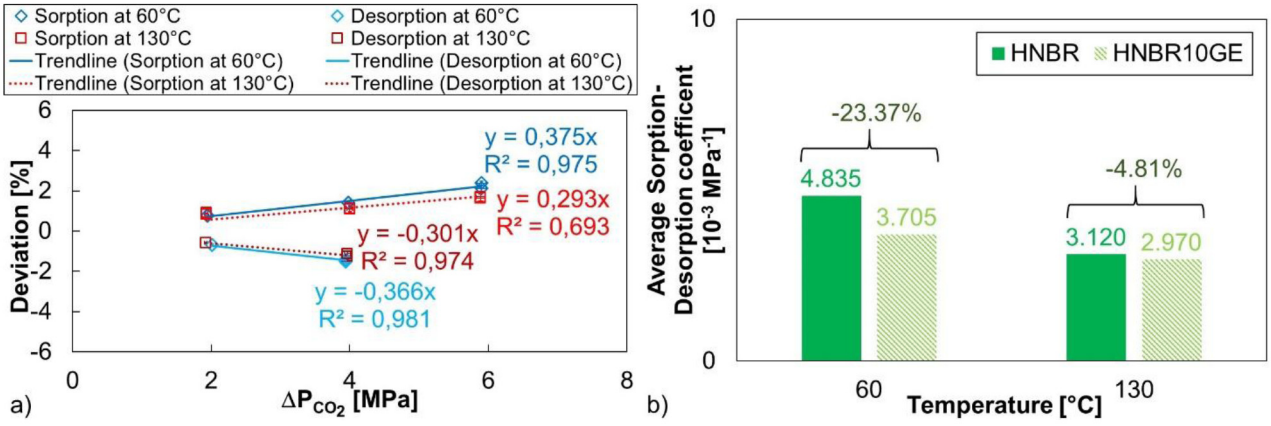

Fig. 5. (a) Deviation as a function of ΔP_{CO_2}. Determination of CO_2 sorption and desorption coefficients at 60 and 130 °C for HNBR10GE; (b) Comparison of the average desorption and desorption coefficients of HNBR and HNBR10GE at 60 and 130 °C.

Fig. 5. *(a) Déviation en fonction de la* ΔP_{CO_2}. *Détermination des coefficients de sorption et de désorption du* CO_2 *à 60 et 130 °C pour le HNBR10GE ; (b) Comparaison de la moyenne des coefficients de sorption et de désorption du HNBR et du HNBR10GE à 60 et 130 °C.*

6 MPa and 130 °C, the HNBR10GE seal seems to open in its parting line, as shown in Figure 6b. Thus, the damage is more significant at 130 °C.

4.5 Effects of 10GE reinforcements on FKM matrix

Figure 7a (Table 4A [see Appendix]) shows the deviations, during sorption and desorption phases, as a function of the pressure variation of CO_2 for the different pressures and both of the temperatures. As in the case of HNBR, a linear regression of the deviation as a function of the pressure is obtained for each configuration and allows to identify the coefficients of sorption and desorption. For FKM10GE at 60 °C, the sorption and desorption coefficients are 5.42×10^{-3} MPa^{-1} and 4.44×10^{-3} MPa^{-1}, respectively. At 130 °C, these coefficients are, respectively, 3.44×10^{-3} MPa^{-1} and 3.51×10^{-3} MPa^{-1} identified for the pressure applied at 2 and 4 MPa since there is no measurement for desorption at 6 MPa. Between 60 and 130 °C, the sorption and desorption coefficients decrease by approximately 36 and 21%, respectively. As noted previously, the determination of the desorption coefficients at 60 and 130 °C, only from the two data at 2 and 4 MPa, is reasonable because these values are very close to those determined for the sorption on the range 2 at 6 MPa.

The average value between sorption and desorption coefficients at both temperatures for both FKM and FKM10GE are compared in Figure 7b. The effect of nanofiller becomes substantial at 60 °C because the sorption-desorption coefficient drops by about 39.31%.

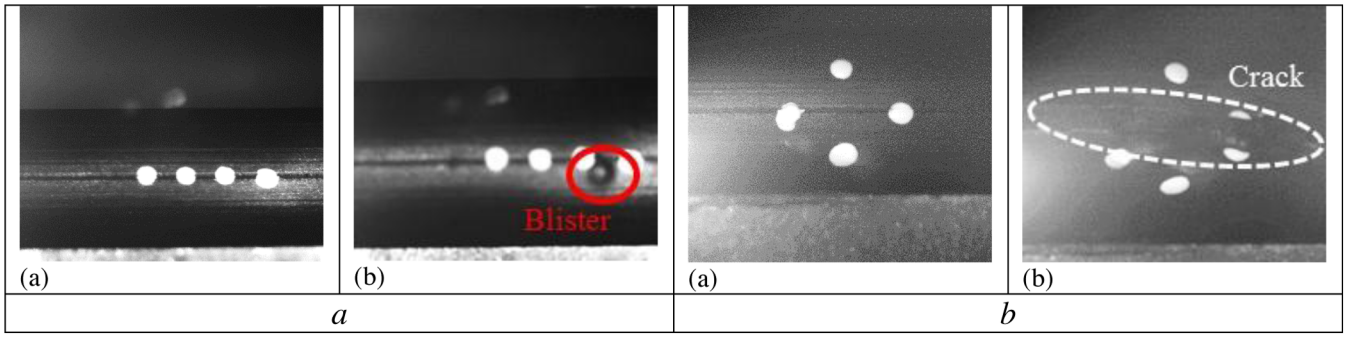

Fig. 6. a. HNBR10GE O-ring [32] (after compression test, 60 °C, and 6 MPa). (a) Photo before decompression $t = 0$ s; (b) Photo during decompression $t = 5$ min. b. HNBR10GE O-ring [32,41] (after compression test, 130 °C, and 6 MPa). (a) Photo before decompression $t = 0$ s; (b) Photo during decompression $t = 7$ min.

Fig. 6. *a. Joint torique HNBR10GE [32] (après essai de compression, 60°C et 6 MPa). (a) Photo avant la décompression $t = 0$ s ; (b) Photo pendant la décompression $t = 5$ min. b. Joint torique HNBR10GE [32,41] (après essai de compression, 130°C et 6 MPa). (a) Photo avant la décompression $t = 0$ s ; (b) Photo pendant la décompression $t = 7$ min.*

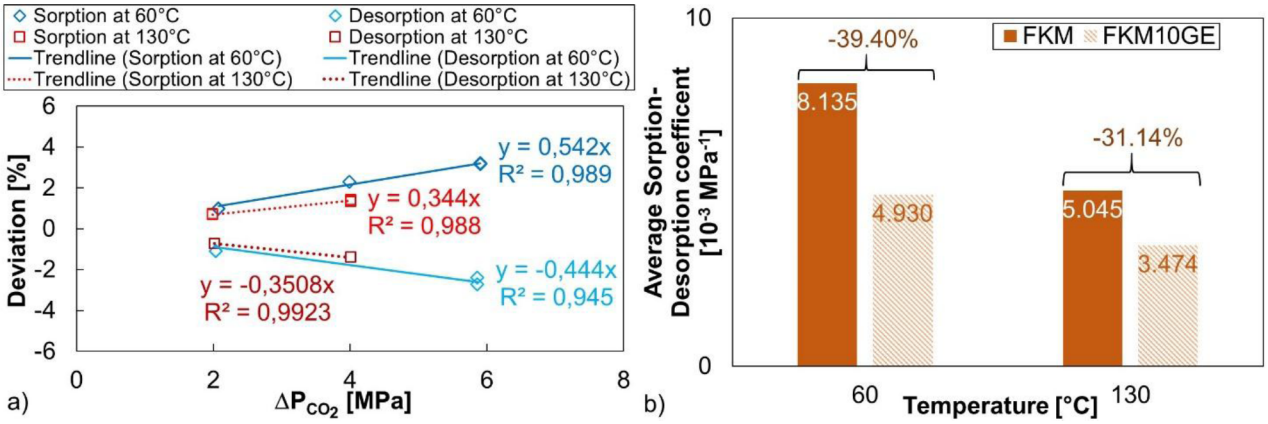

Fig. 7. (a) Deviation as a function of ΔP_{CO_2}. Determination of CO_2 sorption and desorption coefficients at 60 and 130 °C for FKM10GE; (b) Comparison of the average desorption and desorption coefficients of FKM and FKM10GE at 60 and 130 °C.

Fig. 7. *(a) Déviation en fonction de la ΔP_{CO_2}. Détermination des coefficients de sorption et de désorption du CO_2 à 60 et 130°C pour le FKM10GE ; (b) Comparaison de la moyenne des coefficients de sorption et de désorption du FKM et du FKM10GE à 60 et 130°C.*

At 130 °C, the difference narrows to 31.14%, which is much more important than the one observed on HNBR/HNBR10GE. For this family of elastomers, the nanofiller significantly influences this temperature.

Figures 8a–8d show, for different temperature and CO_2 pressure conditions, photos of the initial state and a state at a given time during decompression of the FKM10GE seal. If for both temperatures at 2 MPa, no damage was found during decompression and after observation of the seal at the end of the test, the same cannot be said for the other conditions. Thus at 60 °C, for the 4 and 6 MPa pressures (Figs. 8a and 8c), bubbles (localized swellings) appeared around 3 and 4 min, after the start of decompression. For these same pressures at 130 °C (Figs. 8b and 8d), in addition to the bubbles, ruptures were observed at the markers (on the Parting Line Projection of O-ring).

4.6 Sorption and desorption coefficients under CO_2

Interestingly, the CO_2 desorption shrinking coefficient is plotted as a function of the CO_2 sorption swelling coefficient in HNBR, FKM, HNBR10GE, and FKM10GE, as illustrated in Figure 9a, to evaluate the linear correlation. The error bars for each value are not shown on this graph because they are small, less than 5%. Thus, the size of each marker defines this error interval. The experimental points are very close to the

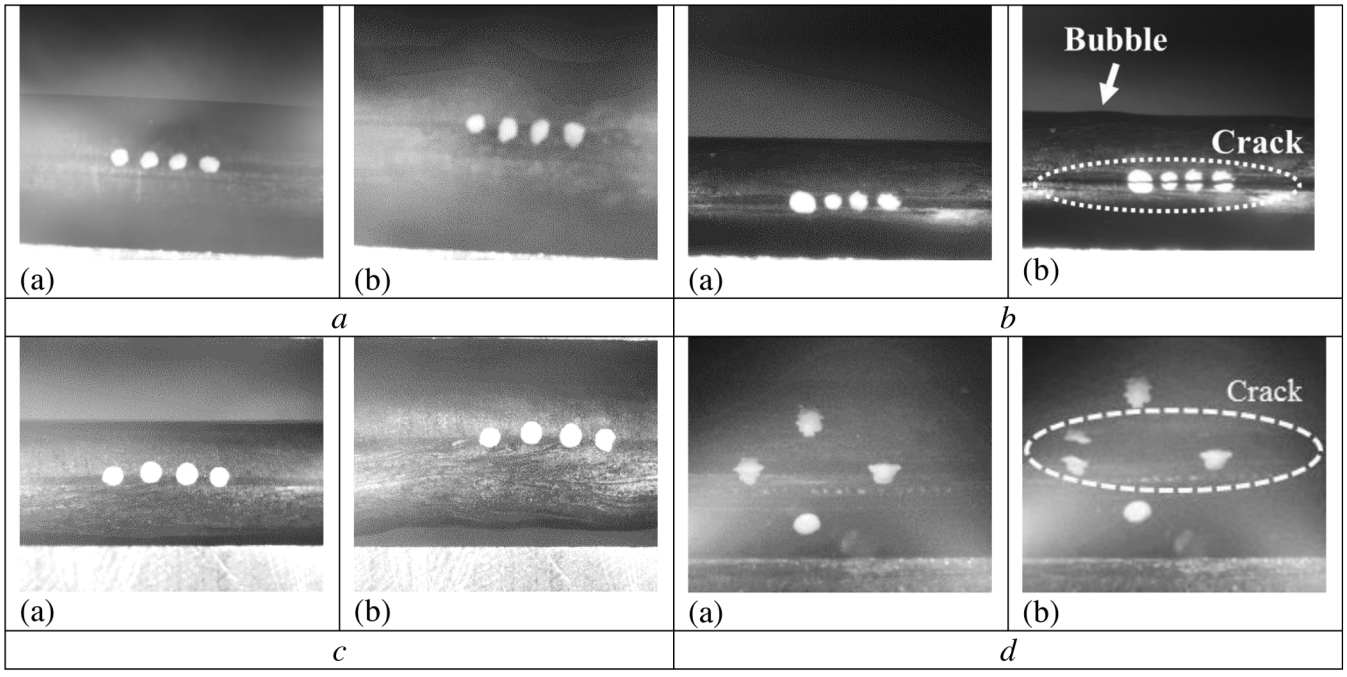

Fig. 8. a. FKM10GE O-ring (after compression test, 60 °C, and 4 MPa). (a) Photo before decompression $t = 0$ s; (b) Photo during decompression $t = 3$ min. b. FKM10GE O-ring (after compression test, 130 °C, and 4 MPa). (a) Photo before decompression $t = 0$ s; (b) Photo during decompression $t = 4$ min. c. FKM10GE O-ring (after compression test, 60 °C, and 6 MPa). (a) Photo before decompression $t = 0$ s; (b) Photo during decompression $t = 4$ min. d. FKM10GE O-ring [32,41] (after compression test, 130 °C, and 6 MPa). (a) Photo before decompression $t = 0$ s; (b) Photo during decompression $t = 7$ min.

Fig. 8. *a. Joint torique FKM10GE (après essai de compression, 60°C et 4 MPa). (a) Photo avant la décompression t = 0 s ; (b) Photo pendant la décompression t = 3 min. b. Joint torique FKM10GE (après essai de compression, 130°C et 4 MPa). (a) Photo avant la décompression t = 0 s ; (b) Photo pendant la décompression t = 4 min. c. Joint torique FKM10GE (après essai de compression, 60°C et 6 MPa). (a) Photo avant la décompression t = 0 s ; (b) Photo pendant la décompression t = 4 min. d. Joint torique FKM10GE [32,41] (après essai de compression, 130°C et 6 MPa). (a) Photo avant la décompression t = 0 s ; (b) Photo pendant la décompression t = 7 min.*

diagonal (dotted line; linear correlation coefficient is equal to 1.0), which shows that the expansion coefficients during the two phases of sorption and desorption are very comparable.

At 130 °C, they are almost identical; a slight deviation is noted at 60 °C for FKM10GE. It seems reasonable to conclude that, for elastic behavior under small strains, the swelling coefficients can be considered undistinguishable to CO_2 sorption and desorption stages, and suggest that during these tests, the effect of the observed post-decompression damage does not affect these couplings. Without considering the accuracy of the measurements, the small deviations observed on FKM10GE and HNBR could be due to a residual deformation at the end of the protocol.

The correlations between the coefficients of thermal expansion and swelling under CO_2 for each material studied at 60 and 130 °C are illustrated in Figure 9b. It seems that a linear relationship exists between these coefficients for these two families of materials. However, this result must be confirmed for other materials to test its generality.

5 Conclusion

After presenting a new technique to measure the swelling of an elastomer during CO_2 sorption and desorption [33], the objective of this work was to validate this approach on other materials. Still, on O-rings to be as close as possible to reality (process), tests were carried out on another elastomer matrix (FKM) and the two reinforced matrices with nanofiller (10GE). The tests were carried out under two temperatures (60 and 130 °C) for different CO_2 sorption pressures (2, 4, and 6 MPa) and vacuum. All these tests first highlighted that this pressure range has almost no impact on the swelling ratio of rubber. The swelling ratio is almost constant with the pressure for each material. On the other hand, the values of swelling are highly dependent on temperature.

Under 6 MPa, the rapid decompression phase leads to a relatively high transient swelling that is the stage before the blistering. The maximum level of swelling during this decompressive phase is higher without a nanofiller in the elastomer.

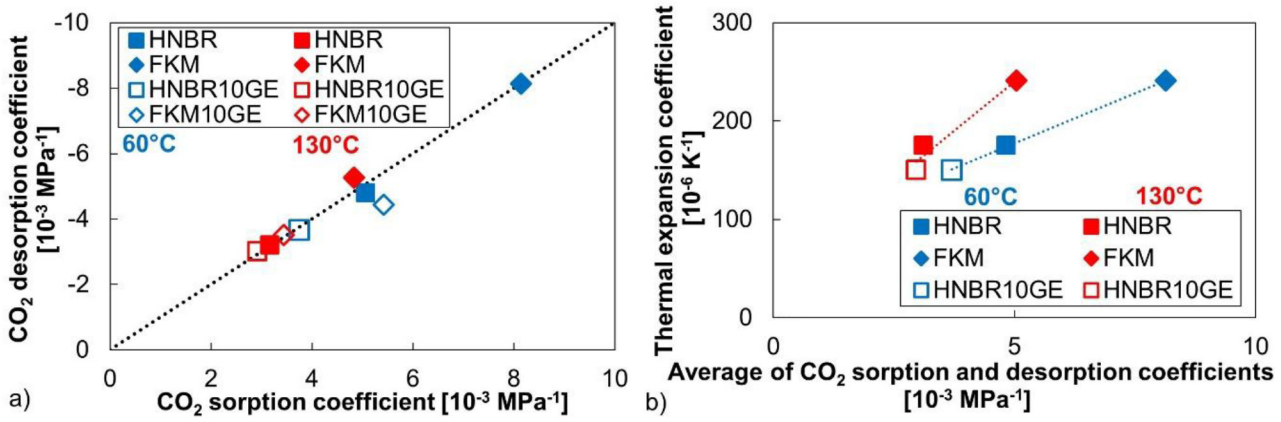

Fig. 9. (a) CO_2 desorption coefficient versus CO_2 sorption coefficient in HNBR, FKM, HNBR10GE, and FKM10GE; (b) Thermal expansion coefficient versus the average of CO_2 sorption and desorption coefficients in HNBR, FKM, HNBR10GE and FKM10GE.

Fig. 9. *(a) Coefficient de désorption CO_2 en fonction du coefficient de sorption CO_2 pour HNBR, FKM, HNBR10GE, and FKM10GE ; (b) Coefficient de dilatation thermique en fonction de la moyenne des coefficients de sorption et de désorption sous CO_2 pour le HNBR, le FKM, le HNBR10GE et le FKM10GE.*

Measurements of the swelling and shrinking ratio in the CO_2 sorption and desorption tests, respectively, highlighted the notable influence of the reinforcements in HNBR and FKM matrices. Finally, between these four materials, it appears that HNBR is the best candidate, as it swells less than FKM under CO_2 pressure and does not damage itself during decompression in this temperature and pressure range.

Credit author statement

Eric Lainé: Conceptualization, Methodology, Validation, Investigation, Writing-original Draft, Writing-Review & Editing, Visualization. Jean-Claude Grandidier: Conceptualization, Writing-Review & Editing, Supervision. Séverine A.E. Boyer: Methodology, Validation, Investigation, Writing-Review & Editing, Visualization. Benoit Omnès: Resources, Writing-Review & Editing, Project administration. Fanny Destaing: Resources, Writing-Review & Editing, Project administration.

Funding

Not applicable.

Conflict of interest

The authors declared no potential conflicts of interest with respect to the research, authorship, and/or publication of this article.

Availability of data and material

Not applicable.

Code availability

Not applicable.

Acknowledgements. We thank Schlumberger Company and Schlumberger Geoservices Company for their Sponsoring in the Citeph project OGSANE (CITEPH-36-2012) and led by the Cetim. In this project, Cetim and Pprime established an R&D collaboration to study the seal behavior with gas. The aim of this private project was the study of the improvement of the performance of rubber seal with nanofiller in rubber in Oil&Gas conditions.
This work was supported by the CPER FEDER project of Région Nouvelle Aquitaine.

Appendix:

Note: The letters S and D, in the second column of each table below, distinguish between the sorption (pressure) and desorption (decompression) phases, respectively.

Table 1A: HNBR Deviations, CO_2 swelling, and CO_2 shrinking coefficients for the different CO_2 sorption and CO_2 desorption tests (2 temperatures and 3 CO_2 pressures).

Test		Temperature	ΔP	DevH14	DevH23	CO_2 swelling/shrinking ratio		
						/DevH14	/DevH23	Average
		(°C)	(MPa)	(%)	(%)	(10^{-3} MPa^{-1})		
1	S	59.93	2.116	1.081	1.075	5.109	5.080	5.095
	D	59.95	−2.093	−0.966	−0.991	4.614	4.734	4.674
2	S	60.22	2.040	1.001	0.981	4.907	4.809	4.858
	D							
3	S	60.34	3.988	1.892	1.876	4.970	4.990	4.980
	D	59.96	−3.966	−1.858	−1.875	4.686	4.727	4.707
4	S	59.80	3.993	2.003	2.019	5.016	5.056	5.035
	D							
5	S	60.32	6.009	3.059	2.938	5.091	4.889	4.990
	D	59.94	−5.993	−2.840	−2.785	4.722	4.630	4.676
6	S	130.05	1.487	/*	0.480	/*	3.228	3.228
	D							
7	S	130.00	2.009	/*	0.683	/*	3.400	3.400
	D	129.81	−1.782	/*	−0.568	/*	3.190	3.187
8	S	130.14	4.125	1.209	1.223	2.931	2.965	2.948
	D	129.36	−4.105	−1.311	−1.313	3.192	3.197	3.195
9	S	130.06	5.756	2.001	1.636	3.476	2.842	3.159
	D	130.03	−5.722	−1.797	−1.779	3.140	3.109	3.125

*Value not retained due to the loss of the image

Table 2A: FKM Deviations, CO_2 swelling, and CO_2 shrinking coefficients for the different CO_2 sorption and CO_2 desorption tests (2 temperatures and 3 CO_2 pressures).

Test		Temperature	ΔP	DevH14	DevH23	CO_2 swelling/shrinking ratio		
						/DevH14	/DevH23	Average
		(°C)	(MPa)	(%)	(%)	(10^{-3} MPa^{-1})		
1	S	59.88	2.163	1.789	1.869	8.271	8.641	8.456
	D	59.41	−2.089	−1.756	−1.672	8.406	8.004	8.205
2	s	60.42	3.985	3.297	3.198	8.274	8.025	8.149
	D	59.31	−4.015	−3.217	−3.345	8.012	8.331	8.172
3	s	59.98	6.131	5.183	4.752	8.454	7.751	8.102
	D	59.30	−6.148	−4.911	−5.051	7.988	8.216	8.102
4	S	131.04	2.051	1.110	1.105	5.412	5.388	5.400
	D	129.73	−2.071	−1.024	−0.947	4.944	4.573	4.759
5	S	130.66	4.019	1.859	1.872	4.626	4.658	4.642
	D	129.68	−4.001	−2.270	−2.171	5.674	5.426	5.550
6	S	130.06	6.060	/	2.948		4.865	4.865
	D	130.05	−6.032	−2.98	−3.29	4.940	5.454	5.197

Table 3A: HNBR10GE Deviations, CO_2 swelling, and CO_2 shrinking coefficients for the different CO_2 sorption and CO_2 desorption tests (2 temperatures and 3 CO_2 pressures).

Test		Temperature	ΔP	DevH14	DevH23	CO_2 swelling/shrinking ratio		
						/DevH14	/DevH23	Average
		(°C)	(MPa)	(%)	(%)	(10^{-3} MPa^{-1})		
1	S	59.91	1.944	0.780	0.769	4.012	3.956	3.984
	D	59.25	−2.010	−0.684	−0.698	3.403	3.473	3.438
2	S	59.84	3.980	1.406	1.409	3.533	3.540	3.536
	D	59.29	−3.945	−1.408	−1.524	3.569	3.863	3.716
3	S	58.65	5.899	2.379	2.122	4.033	3.597	3.815
	D	59.61	−5.842	/	/			
4	S	131.02	1.927	0.840	0.903	4.359	4.686	4.523
	D	130.11	−1.823	−0.583	−0.584	−3.032	−3.037	3.034
5	S	130.55	4.001	1.093	1.132	2.732	2.829	2.781
	D	129.53	−3.967	−1.122	−1.263	−2.828	−3.184	3.006
6	S	130.07	5.888	1.698	1.639	2.884	2.784	2.834
	D							

Table 4A: FKM10GE Deviations, CO_2 swelling, and CO_2 shrinking coefficients for the different CO_2 sorption and CO_2 desorption tests (2 temperatures and 3 CO_2 pressures).

Test		Temperature	ΔP	DevH14	DevH23	CO_2 swelling/shrinking ratio		
						/DevH14	/DevH23	Average
		(°C)	(MPa)	(%)	(%)	(10^{-3} MPa^{-1})		
1	S	59.92	2.077	1.016	0.976	4.892	4.699	4.795
	D	59.44	−2.035	−1.074	−1.072	5.278	5.268	5.273
2	S	59.79	3.987	2.292	2.764	5.749	6.933	6.341
	D			/	/			
3	S	58.67	5.903	3.180	3.220	5.387	5.455	5.421
	D	59.62	−5.861	−2.713	−2.374	4.629	4.051	4.340
4	S	130.67	1.994	0.687	0.715	3.445	3.586	3.516
	D	130.08	−2.020	−0.868	−0.878	3.619	3.658	3.639
5	S	130.83	4.010	1.326	1.422	3.307	3.546	3.426
	D	129.65	−4.010	−1.380	−1.395	3.441	3.479	3.460
6	S	130.06	6.025	2.757	2.621	4.576	4.350	4.463
	D							

References

1. S. Ahmed, S. Salehi, C.P. Ezeakacha, et al., Experimental investigation of elastomers in downhole seal elements: Implications for safety, Polym. Test. **76**, 350–364 (2019), https://doi.org/10.1016/j.polymertesting.2019.03.041
2. M. Najipoor, L. Haroonabadi, A. Dashti, Assessment of failures of nitrile rubber vulcanizates in rapid gas decompression (RGD) testing: Effect of physico-mechanical properties, Polym. Test. **72**, 377–385 (2018), https://doi.org/10.1016/j.polymertesting.2018.11.002
3. S. Ahmed, H. Patel, S. Salehi, Numerical modeling and experimental study of elastomer seal assembly in downhole wellbore equipment: Effect of material and chemical swelling, Polym. Test. **89**, 1–15 (2020), https://doi.org/10.1016/j.polymertesting.2020.106608
4. B. Alcock, T.A. Peters, A. Tiwari, The effect of hot air exposure on the mechanical properties and carbon dioxide permeability of hydrogenated nitrile butadiene rubber (HNBR) with varying carbon black content, Polym. Test. **82**, 1–10 (2020), https://doi.org/10.1016/j.polymertesting.2019.106273
5. B. Alcock, T.A. Peters, R.H. Gaarder, et al., The effect of hydrocarbon ageing on the mechanical properties, apparent crosslink density and CO_2 diffusion of a hydrogenated nitrile butadiene rubber (HNBR), Polym. Test. **47**, 22–29 (2015), https://doi.org/10.1016/j.polymertesting.2015.07.007
6. T. Grelle, D. Wolff, M. Jaunich, Temperature-dependent leak tightness of elastomer seals after partial and rapid release of compression, Polym. Test. **48**, 44–49 (2015), https://doi.org/10.1016/j.polymertesting.2015.09.009
7. S.Z. Qamar, M. Akhtar, T. Pervez, et al., Mechanical and structural behavior of a swelling elastomer under compressive loading, Materials & Design **45**, 487–496 (2013), http://dx.doi.org/10.1016/j.matdes.2012.09.020
8. B.J. Briscoe, T. Savvas, C.T. Kelly, Explosive decompression failure of rubbers – A review of the origins of pneumatic stress-induced rupture in elastomers, Rubber Chem. Technol. **67**, 384–416 (1994), https://doi.org/10.5254/1.3538683
9. B.J. Briscoe, C.T. Kelly, The effect of structure on gas solubility and gas induced dilation in a series of poly (urethane) elastomers, Polymer **37**, 3405–3410 (1996), https://doi.org/10.1016/0032-3861(96)88488-6
10. Z. Major, R.W. Lang, Characterization of the fracture behavior of NBR and FKM grade elastomers for oilfield applications, Eng. Fail. Anal. **17**, 701–711 (2010), https://doi.org/10.1016/j.engfailanal.2009.08.004
11. O.M. Davies, J.C. Arnold, S. Sulley, The mechanical properties of elastomers in high-pressure CO_2, J. Mat. Sci. **34**, 417–422 (1999), https://doi.org/10.1023/A:1004442614090
12. L. Ansaloni, B. Alcock, T.A. Peters, Effects of CO_2 on polymeric materials in the CO_2 transport chain: A review, Int. J. GreenH. Gas Control. **94**, 1–15 (2020), https://doi.org/10.1016/j.ijggc.2019.102930
13. J.C. Legros, A. Mialdun, P. Strizhak, et al., Permeation of supercritical CO_2 through perfluoroelastomers, J. Supercrit. Fluids **126**, 1–13 (2017), https://dx.doi.org/10.1016/j.supflu.2017.02.022
14. L. Haroonabadi, A. Dashti, M. Najipour, Investigation of the effect of thermal aging on rapid gas decompression (RGD) resistance of nitrile rubber, Polym. Test. **67**, 37–45 (2018), https://doi.org/10.1016/j.polymertesting.2018.02.014
15. X. Chen, H.A. Salem, R. Zonoz, CO_2 Solubility and diffusivity and rapid gas decompression resistance of elastomers containing CNT, Rubber Chem. Technol. **90**, 562–574 (2017), https://doi.org/10.5254/rct.17.83726
16. B. Bonavoglia, G. Storti, M. Morbidelli, et al., Sorption and swelling of semicrystalline polymers in supercritical CO_2, J. Polym. Sci. Part B: Polym. Phys. **44**, 1531–1546 (2006), https://doi.org/10.1002/polb.20799
17. S. Shenoy, D. Woerdeman, R. Sebra, et al., Quantifying polymer swelling employing a linear variable differential transformer: CO_2 effects on SBS triblock copolymer, Macromol. Rapid Commun. **23**, 1130–1133 (2002), https://doi.org/10.1002/marc.200290007
18. B. Schrittesser, G. Pinter, T. Schwarz, et al., Rapid gas decompression performance of elastomers – A study of influencing testing parameters, Proc. Struct. Integr. **2**, 1746–1754 (2016), https://doi.org/10.1016/j.prostr.2016.06.220
19. J. Dubois, E. Grau, T. Tassaing, et al., On the CO_2 sorption and swelling of elastomers by supercritical CO_2 as studied by in situ high pressure FTIR microscopy, J. Supercrit. Fluids **131**, 150–156 (2018), https://doi.org/10.1016/j.supflu.2017.09.003
20. A. Rajendran, A. Bonavoglia, B. Forrer, et al., Simultaneous measurement of swelling and sorption in a supercritical CO_2-poly(methyl methacrylate) system, Ind. Eng. Chem. Res. **44**, 2549–2560 (2005), https://doi.org/10.1021/ie049523w
21. F. Daou, C.R. de Miranda, J.L. de Oliveira, et al., Swelling of elastomers in CO_2 environment: Testing methodology and experimental data, in: SPE Latin America and Caribbean Petroleum Engineering Conference, Maracaibo, Venezuela SPE-169277-MS, (2014)
22. K.J. Thurecht, D.J.T. Hill, A.K. Whittaker, Equilibrium swelling measurements of network and semicrystalline polymers in supercritical carbon dioxide using high pressure NMR, Macromolecules **38**, 3731–3737 (2005), https://doi.org/10.1021/ma0503108
23. S.K. Goel, E.J. Beckman, Modelling the swelling of cross-linked elastomers by supercritical fluids, Polymer **33**, 5032–5039 (1992), https://doi.org/10.1016/0032-3861(92)90054-Z
24. S. Salehi, C.P. Ezeakacha, G. Kwatia, et al., Performance verification of elastomer materials in corrosive gas and liquid conditions, Polym. Test. **75**, 48–63 (2019), https://doi.org/10.1016/j.polymertesting.2019.01.015
25. S. Hilic, S.A.E. Boyer, A.A.H. Padua, et al., Simultaneous measurement of the solubility of nitrogen and carbon dioxide in polystyrene and of the associated polymer swelling, J. Polym. Sci. Part B: Polym. Phys. **39**, 2063–2070 (2001), https://doi.org/10.1002/polb.1181
26. R.M.H. Felder, Permeation, diffusion, and sorption of gases and vapors, in: R.A. Fava, ed., Methods Exp. Physics, Part C: Polymer Physics, Academic Press, New York, 1980
27. Y. Kamiya, K. Mizoguchi, K. Terada, et al., CO_2 sorption and dilation of poly(methyl methacrylate), Macromolecules **31**, 472–478 (1998), https://doi.org/10.1021/ma970456+
28. N.H. Brantley, S.G. Kazarian, C.A. Eckert, In situ FTIR measurement of carbon dioxide sorption into poly(ethylene terephthalate) at elevated pressures, J. Appl. Polym. Sci. **77**, 764–775 (2000), https://doi.org/10.1002/(SICI)1097-4628(20000725)77:4<764
29. R.G. Wissinger, M.E. Paulaitis, Swelling and sorption in polymer-CO_2 mixtures at elevated pressures, J. Polym. Sci Part B: Polym. Phys. **25**, 2497–2510 (1987), https://doi.org/10.1002/polb.1987.090251206

30. J.R. Royer, J.M. De Simone, S.A. Khan, Carbon dioxide-induced swelling of poly(dimethylsiloxane), Macromolecules 32, 8965–8973 (1999), https://doi.org/10.1021/ma9904518
31. D.H. Ender, Elastomeric seals, Chem. Tech. **16**, 52–57 (1986)
32. E. Lainé, J.C. Grandidier, G. Benoit, et al., Effects of sorption and desorption of CO_2 on the thermomechanical experimental behavior of HNBR and FKM O-rings – Influence of nanofiller-reinforced rubber, Polym. Test. **75**, 298–311 (2019), https://doi.org/10.1016/j.polymertesting.2019.02.010
33. E. Lainé, J.C. Grandidier, G. Benoit, et al., Non-contact method used to determine the swelling/shrinking coefficients under CO_2 sorption/desorption on an HNBR O-ring – Study of coupling with temperature and pressure, Polym. Test. **85**, 1–16 (2020), https://doi.org/10.1016/j.polymertesting.2020.106411
34. S. Castagnet, J.C. Grandidier, M. Comyn, et al., Effect of long-term hydrogen exposure on the mechanical properties of polymers used for pipes and tested in press urized hydrogen, Int. J. Press. Vessels Pip. **89**, 203–209 (2012), https://doi.org/10.1016/j.ijpvp.2011.11.008
35. S.A.E. Boyer, M. Gerland, S. Castagnet, Gas environment effect on cavitation damage in stretched PolyVinylidene Fluoride, Polym. Eng. Sci. **54**, 2139–2146 (2014), https://doi.org/10.1002/pen.23759
36. Z. Sun, G. Benoit, C. Moriconi, et al., Fatigue crack propagation under gaseous hydrogen in a precipitation-hardened martensitic stainless steel, Int. J. Hydrogen Energy **36**, 8641–8644 (2011), https://doi.org/10.1016/j.ijhydene.2011.04.094
37. S. Castagnet, J.C. Grandidier, M. Comyn, et al., Mechanical testing of polymers into pressurized hydrogen: tension, creep and ductile fracture, Exp. Mech. **52**, 229–239 (2012)
38. G. Benoit, S.A.E. Boyer, S. Castagnet, et al., Mechanical testing in press urized hydrogen and carbon dioxide, in: The 10th BSSM International Conference on Advances in Experimental Mechanics, September 1st–3rd, Edinburg, Scotland, 2015
39. Nace Standard TM0192-98, Evaluating elastomeric materials in carbon dioxide decompression environments, 1998
40. Norsok Stand, M-710 Rev. 3 Qualification of non-metallic sealing materials and manufacturers, 2014
41. E. Lainé, J.C. Grandidier, G. Benoit, et al., Mechanical characterization under CO_2 of HNBR and FKM grade elastomers for oilfield applications – Effects of 10GE reinforcements, Constitutive Models for Rubber X. Lion & Johlitz Eds, Talyor & Francis Group London, 231–236 (2017)

Cite this article as: Eric Lainé, Jean-Claude Grandidier, Séverine A.E. Boyer, Benoit Omnès, Fanny Destaing, Identification of swelling/shrinking coefficients under CO_2 on an FKM O-ring – Comparison with HNBR and influence of reinforcements on the matrices, Matériaux & Techniques **110**, 303 (2022)